Systems/Circuits

FABP3 in the Anterior Cingulate Cortex Modulates the Methylation Status of the Glutamic Acid Decarboxylase$_{67}$ Promoter Region

Yui Yamamoto,[1,2] Hiroyuki Kida,[3] Yoshiteru Kagawa,[1] Yuki Yasumoto,[1] Hirofumi Miyazaki,[1] Ariful Islam,[1] Masaki Ogata,[1,2] Yuchio Yanagawa,[4] Dai Mitsushima,[3] Kohji Fukunaga,[5] and Yuji Owada[1]

[1]Department of Organ Anatomy, Tohoku University, Sendai 980-8575, Japan, [2]Department of Anatomy, Tohoku Medical and Pharmaceutical University, Sendai 983-8536, Japan, [3]Department of System Neuroscience, Yamaguchi University, Ube 755-8505, Japan, [4]Department of Genetic and Behavioural Neuroscience, Gunma University, Maebashi 371-8511, Japan, and [5]Department of Pharmacology, Graduate School of Pharmaceutical Sciences, Tohoku University, Sendai 980-8578, Japan

Polyunsaturated fatty acids (PUFAs) are essential for brain development and function. Increasing evidence has shown that an imbalance of PUFAs is associated with various human psychiatric disorders, including autism and schizophrenia. Fatty acid-binding proteins (FABPs), cellular chaperones of PUFAs, are involved in PUFA intracellular trafficking, signal transduction, and gene transcription. In this study, we show that FABP3 is strongly expressed in the GABAergic inhibitory interneurons of the male mouse anterior cingulate cortex (ACC), which is a component of the limbic cortex and is important for the coordination of cognitive and emotional behaviors. Interestingly, *Fabp3* KO male mice show an increase in the expression of the gene encoding the GABA-synthesizing enzyme glutamic acid decarboxylase 67 (*Gad67*) in the ACC. In the ACC of *Fabp3* KO mice, *Gad67* promoter methylation and the binding of methyl-CpG binding protein 2 (MeCP2) and histone deacetylase 1 (HDAC1) to the *Gad67* promoter are significantly decreased compared with those in WT mice. The abnormal cognitive and emotional behaviors of *Fabp3* KO mice are restored by methionine administration. Notably, methionine administration normalizes *Gad67* promoter methylation and its mRNA expression in the ACC of *Fabp3* KO mice. These findings demonstrate that FABP3 is involved in the control of DNA methylation of the *Gad67* promoter and activation of GABAergic neurons in the ACC, thus suggesting the importance of PUFA homeostasis in the ACC for cognitive and emotional behaviors.

Key words: ACC; FABP3; GABA; GAD67; parvalbumin; PUFA

Significance Statement

The ACC is important for emotional and cognitive processing. However, the mechanisms underlying its involvement in the control of behavioral responses are largely unknown. We show the following new observations: (1) FABP3, a PUFA cellular chaperone, is exclusively expressed in GABAergic interneurons in the ACC; (2) an increase in *Gad67* expression is detected in the ACC of *Fabp3* KO mice; (3) the *Gad67* promoter is hypomethylated and the binding of transcriptional repressor complexes is decreased in the ACC of *Fabp3* KO mice; and (4) elevated *Gad67* expression and abnormal behaviors seen in *Fabp3* KO mice are mostly recovered by methionine treatment. These suggest that FABP3 regulates GABA synthesis through transcriptional regulation of *Gad67* in the ACC.

Introduction

The anterior cingulate cortex (ACC) is a component of the limbic system. The ACC is particularly important for emotional and cognitive processing (Bush et al., 2000) and is reciprocally connected to areas important for emotional conflict (e.g., the

amygdala [AM]), working memory (e.g., the hippocampus), cognition (e.g., the PFC), and pain processing (e.g., the hypothalamus) (Devinsky et al., 1995; Bush et al., 2000). In rodents and nonhuman primates, the ACC has been associated with the regulation of aversive behavior to noxious stimuli (Johansen et al., 2001; Johansen and Fields, 2004), reward-based decision-making (Amemori and Graybiel, 2012), and remote memory (Frankland et al., 2004) based on pharmacological inactivation, microstimulation, and lesion studies. In humans, studies using fMRI indicate that hypoactivity of the ACC is associated with several neuropsychiatric diseases, including attention deficit hyperactivity disorder (Bush et al., 1999), conduct disorder (Stadler et al., 2007), and autism spectrum disorders (Di Martino et al., 2009). However, the mechanisms that underlie the involvement of the ACC in the control of behavioral responses and the pathology of neuropsychiatric diseases are largely unknown.

Fatty acid-binding proteins (FABPs) are intracellular, low-molecular-weight (14–15 kDa) polypeptides that are key molecules in the uptake, transport, and storage of long-chain fatty acids (Furuhashi and Hotamisligil, 2008; Liu et al., 2008). To date, 10 members of the FABP family have been recognized in mammals; these are expressed in different organs, tissues, and cell types with spatial heterogeneity. FABP3, FABP5, and FABP7 are expressed in the CNS (Owada et al., 1996): FABP5 and FABP7 are predominantly expressed in glial cells, whereas FABP3 is expressed in various types of neurons in the adult brain (Owada et al., 1996).

FABP3, which preferentially binds to n-6 polyunsaturated fatty acids (PUFAs), such as arachidonic acid, is expressed in the brain, heart, skeletal muscle, lactating mammary gland, and placenta (Watanabe et al., 1993; Islam et al., 2014). We recently determined that *Fabp3* KO mice show enhanced haloperidol-induced catalepsy (Shioda et al., 2010) and α-synuclein oligomerization in the basal ganglia (Shioda et al., 2014), which suggests a role of FABP3 in the control of dopaminergic function, as well as its involvement in the pathology of Parkinson's disease. Furthermore, we also showed that *Fabp3* KO mice exhibit decreased novelty-seeking behavior (Shimamoto et al., 2014), which is closely associated with ACC function alterations (Weible et al., 2009). However, it remains unclear how FABP3 regulates ACC-related behaviors and synaptic functions in the ACC.

Changes in DNA methylation status in the PFC, including the ACC, affect various behaviors. Region-specific overexpression or knockdown of DNA methyltransferase (DNMT) in the mPFC of mice renders them behaviorally anxiolytic or anxiogenic, respectively (Elliott et al., 2016). Moreover, chronic intra-ACC infusion of DNMT inhibitors after contextual fear training prevents the expression of remote memories via a decrease in the DNA methylation of the memory suppressor gene in the ACC (Miller et al., 2010; Bali et al., 2011). This evidence suggests that DNA methylation is critical for emotional behavior and remote memory formation. However, the molecular basis and significance of the epigenetic control of ACC function remain unknown.

In the present study, we examined the detailed localization of FABP3 in the ACC of adult mice and explored its role using *Fabp3* KO mice. We determined that FABP3 was expressed by parvalbumin-positive (PV$^+$) GABAergic interneurons in the ACC and that *Fabp3* KO mice exhibited increased glutamic acid decarboxylase 67 (*Gad67*) mRNA levels in the ACC. Moreover, *Gad67* promoter hypomethylation in the ACC of *Fabp3* KO mice was successfully restored following methyl donor treatment. Our findings demonstrate that FABP3 plays a critical role in cognitive and emotional behaviors through its regulation of *Gad67* promoter methylation in the ACC.

Materials and Methods

Animals. Twelve-week-old C57BL/6 WT, homozygous *Fabp3* KO (Binas et al., 1999), and *Gad67-GFP* knock-in mice (Tamamaki et al., 2003) were used in this study. Mice were housed under climate-controlled conditions with a 12 h light/dark cycle and were provided standard food and water *ad libitum*. All experimental protocols were approved by the Ethics Committee for Animal Experimentation of the Yamaguchi University Graduate School of Medicine and Tohoku University Graduate School of Medicine and were performed according to the Guidelines for Animal Experimentation of each institute under the law and notification requirements of the Japanese government.

RT-PCR and qRT-PCR. Areas that encompass the ACC were carefully dissected from WT and *Fabp3* KO mice (12-week-old male mice, $n = 6$ per genotype) and were immediately frozen in liquid nitrogen. Total RNA was isolated using the RNeasy Mini Kit (QIAGEN) and reverse-transcribed using the First Strand cDNA Synthesis Kit (Roche Diagnostics). For RT-PCR analysis, the following primers were used: *Fabp3*, 5′-CATGAAGTCACTCGGTGTGG-3′ (forward) and 5′-TGCCATGAGTGAGAGTCAGG-3′ (reverse); and β-Actin, 5′-CAGGAGATGGCCACTGCCGCA-3′ (forward) and 5′-CTCCTTCTGCATCCTGTCAGCA-3′ (reverse). The PCR program was as follows: 94°C denaturation for 4 min, followed by 25 cycles of 94°C for 1 min, 60°C for 1 min, and 72°C for 1 min. PCR products were electrophoresed on a 1.5% agarose gel, and gel images were digitally captured with the BioDoc-It Imaging System (UVP). For qPCR analysis, the gene expression of each cDNA sample was analyzed using TaqMan Probe reagent on a Step One Plus thermal cycler (Applied Biosystems) according to the manufacturer's protocol. The following TaqMan probes were used: *Gad67*, Mm00725661_s1; *Fabp3*, Mm00725661_s1; and *Gapdh*, Mm 03302249_g1. Gene expression levels were calculated and standardized using the ΔΔCt method and *Gapdh* gene expression levels as an internal control.

Histological examination. Mice were transcardially perfused with PBS, pH 7.4, followed by perfusion with 4% PFA in PBS under isoflurane anesthesia. The brains were removed, postfixed with the same fixative overnight at 4°C, cryoprotected with graded sucrose (10%, 20%, and 30% for ∼12 h each), and stored at −80°C. Serial coronal sections 40 μm thick were prepared using a CM1850 cryostat (Leica Microsystems).

For immunofluorescence staining, the sections were incubated as follows: 30 min in PBS, pH 7.4, containing 0.3% Triton X-100; 1 h in PBS containing 5% normal goat serum (blocking solution); and overnight with various primary antibodies in blocking solution. The primary antibodies included mouse monoclonal antibodies against FABP3 (1:200, Hycult Biotechnology HM2016, RRID:AB_533050); rabbit polyclonal antibodies against neurogranin (Ng, 1:2000, Millipore AB5620, RRID:AB_91937); rabbit polyclonal antibodies against PV (1:2000, Abcam ab11427, RRID:AB_298032); rat monoclonal antibodies against somatostatin (SOM, 1:50, Millipore MAB354, RRID:AB_2255365); and rabbit polyclonal antibodies against calretinin (CR, 1:2000, Swant CR7697, RRID:AB_2619710). The sections were subsequently incubated with AlexaFluor-488- or 594-conjugated secondary antibody (1:500, Invitrogen) against mouse IgG, rabbit IgG, or rat IgG. After counterstaining of nuclei with DAPI, the slides were covered with Fluoromount (Diagnostic BioSystems K024) and observed under an LSM780 confocal laser microscope (Carl Zeiss). The position of the ACC was identified based on the atlas of Paxinos and Franklin (2004).

Western blot analysis. Western blotting analysis was performed as previously described (Yamamoto et al., 2009, 2013). Mouse brains were rapidly removed and perfused in ice-cold buffer (0.32 M sucrose, 20 mM Tris-HCl, pH 7.4) for 3 min. The ACC, mPFC, or AM tissues were dissected and homogenized in buffer containing 50 mM Tris-HCl, pH 7.4, 0.5% Triton X-100, 4 mM EGTA, 10 mM EDTA, 1 mM Na$_3$VO$_4$, 40 mM sodium pyrophosphate, 50 mM NaF, 100 nM calyculin A, 50 μg/ml leupeptin, 25 μg/ml pepstatin A, 50 μg/ml trypsin inhibitor, and 1 mM DTT. Supernatants were obtained after centrifugation, and the protein concentration was determined using a BCA Protein Assay Kit (Thermo Fisher Scientific). Samples were boiled for 3 min in Laemmli sample

buffer and subjected to SDS-PAGE. Proteins were transferred onto an Immobilon PVDF membrane (Millipore) for 2 h at 70 V; the membrane was treated with TTBS solution (50 mM Tris-HCl, pH 7.5, 150 mM NaCl, and 0.1% Tween 20) containing 2.5% BSA for 1 h at 25°C and incubated overnight at 4°C with primary antibody solution. The following antibodies were used: mouse monoclonal anti-GAD67 (1:2000, Sigma-Aldrich G5419, RRID:AB_261978), anti-GAD65 (1:10,000, Sigma-Aldrich SAB4200232, RRID:AB_10762670), anti-gephyrin (1:5000, Synaptic Systems 147 111, RRID:AB_887719), anti-synaptophysin (1:1000, Sigma-Aldrich S5768, RRID:AB_477523), anti-phospho-calcium/calmodulin-dependent protein kinase IV (CaMKIV; 1:1000) (Kasahara et al., 1999), anti-total-CaMKIV (1:1000) (Kasahara et al., 1999), anti-β-actin (1:5000, Santa Cruz Biotechnology sc-47778, RRID:AB_2714189), anti-β-tubulin (1:5000, Santa Cruz Biotechnology sc-58886, RRID: AB_793550), rabbit monoclonal anti-BDNF (1:10,000, Abcam ab108319, RRID:AB_10862052), rabbit polyclonal anti-vesicular GABA transporter (VGAT; 1:1000, Synaptic Systems 131003, RRID: AB_887869), anti-postsynaptic density-95 (PSD95; 1:1000, Cell Signaling Technology 3450, RRID:AB_2292883), anti-methyl-CpG binding protein 2 (MeCP2; 1:1000, Abcam ab2828, RRID:AB_2143853), anti-histone deacetylase 1 (HDAC1; 1:1000, Millipore 17-101199, RRID:AB_11203477), anti-phospho-cAMP-responsive-element-binding protein (CREB; 1:1000, Millipore 05-807, RRID:AB_310017), anti-FABP3 (1:500, ProteinTech 10676-1-AP, RRID:AB_2102309), guinea pig polyclonal anti-vesicular glutamate transporter 1 (VGLUT1; 1:5000, Millipore AB5905, RRID:AB_2301751), and anti-GABA$_A$ receptor α1 subunit (GABA$_A$R, 1:10,000, Frontier Institute GP-Af440, RRID:AB_2571572). After washing with TTBS, the membrane was treated with secondary antibody, and the reaction was analyzed using Imager 600 (GE Healthcare).

Measurement of brain GABA, dopamine (DA), serotonin (5-HT), and glutamate concentrations. Brain GABA, DA, and 5-HT concentrations were determined using commercial ELISA kits (BA E-2600; BA E-5900; BA E-5300, LDN) according to the manufacturer's instructions. The mice were killed by decapitation, and the ACC, mPFC, and AM were rapidly dissected on an ice-cold plate, frozen, and stored at −80°C until use. On the day of analysis, total proteins from WT and *Fabp3* KO mice were extracted using lysis buffer (10 mM Tris, pH 7.4, 5 mM EDTA, 0.1% SDS, 0.5% deoxycholate, and 0.5% NP40). Protein concentrations were measured using the BCA Protein Assay Kit (Thermo Fisher Scientific). For ELISA measurements, the sample volume was normalized using 100 μg of protein.

Microdialysis studies were performed as described previously (Shioda et al., 2010; Yamamoto et al., 2013). A guide cannula (AG-4, Eicom) was inserted into the ACC under anesthesia (1.5% halothane, Takeda Chemical Industries) at the position 1 mm anterior to the bregma, 0.5 mm lateral to the midline, and 0.5 mm ventral from the dura surface according to the atlas of Paxinos and Franklin (2004). Twenty-four hours after recovery, microdialysis probes (A-I-4-02, dialysis membrane: 2 mm long, outer diameter: 0.22 mm, Eicom) were inserted. Microdialysis was performed using a fully automated online system in HTEC-500GAA (Eicom) for glutamate analyses in freely moving mice. The microdialysis probe was perfused with Ringer's solution (1.3 mM CaCl$_2$, 3 mM KCl, 146 mM NaCl, and 1 mM MgSO$_4$) at a 2.0 μl/min flow rate using a microsyringe pump (ESP-64, Eicom) over the entire period. The KCl-induced glutamate concentration was measured in the acute phase with an increased KCl content (1.3 mM CaCl$_2$, 146 mM KCl, 3 mM NaCl, and 1 mM MgSO$_4$) at a flow rate of 2.0 μl/min using a microsyringe pump (ESP-64, Eicom) for a 20 min period and was subsequently replaced with normal Ringer's solution. Dialysates were collected every 19.5 min in the sample loop of an auto-injector (EAS-20, Eicom) and then analyzed by HPLC with electrochemical detection (HTEC-500, Eicom).

Cells and transfection. Mouse neuroblastoma Neuro-2A (ATCC CCL-131, RRID:CVCL_0470) cells were maintained in DMEM (Sigma-Aldrich) supplemented with 2 mM L-glutamate and 10% FBS at 37°C under 5% CO$_2$. Neuro-2a cells were plated in 35 mm dishes, cultured in standard medium for 48 h, and transfected using Lipofectamine 2000 (Invitrogen) for plasmid transfection and Lipofectamine RNAiMAX (Invitrogen) for siRNA transfection according to the manufacturer's protocols. The culture medium was changed to the standard medium, and cells were cultured for an additional 24 h. Cell differentiation was initiated by serum starvation. After 24 h of incubation, cells were harvested and subjected to qPCR, Western blotting, and *S*-adenosine methionine (SAM) ELISA.

Electrophysiological recordings. Brain slices (350 μm) containing the ACC were prepared from 10- to 12-week-old mice as previously described (Mitsushima et al., 2013; Ebrahimi et al., 2016; Kida et al., 2016). The slices were incubated in a physiological solution containing the following: 118 mM NaCl, 2.5 mM KCl, 26 mM NaHCO$_3$, 1 mM NaH$_2$PO$_4$, 10 mM glucose, 4 mM MgCl$_2$, 4 mM CaCl$_2$, pH 7.4 (saturated with 95% O$_2$/5% CO$_2$). For miniature response recordings, we used a physiological solution containing 0.5 μM tetrodotoxin to block Na$^+$ channels. Patch-recording pipettes (4–7 MΩ) were filled with modified intracellular solution (127.5 mM cesium methane sulfonate, 7.5 mM CsCl, 10 mM HEPES, 2.5 mM MgCl$_2$, 4 mM Na$_2$ATP, 0.4 mM Na$_3$GTP, 10 mM sodium phosphocreatine, 0.6 mM EGTA, pH 7.25) to adjust the reversal potential of the GABA$_A$ receptor response. Whole-cell recordings were obtained from pyramidal neurons in the ACC with an Axopatch-700B amplifier (Molecular Devices). We analyzed the frequency and amplitude of mEPSCs and mIPSCs >10 pA. After recording, we confirmed that mEPSCs and mIPSCs were completely abolished by 10 μM CNQX (Sigma-Aldrich) and 10 μM bicuculline methiodide (Sigma-Aldrich), respectively.

Chromatin immunoprecipitation (ChIP). ChIP assays were performed using the Magna ChIP G Tissue Kit (Millipore) according to the manufacturer's protocol. Briefly, after crosslinking with 1% formaldehyde, chromatin was sheared using the ChIP-IT Express Enzymatic Shearing Kit (Active Motif) into fragments of 200–1000 bp. Sheared chromatin was immunoprecipitated using Protein G magnetic beads and conjugated with 5 μg ChIP-grade antibodies against MeCP2 (Abcam) or HDAC1 (Millipore) or rabbit IgG control antibodies (Active Motif). Bound and unbound sheared cross-linked chromatin was subsequently eluted according to the manufacturer's instructions. For identification of the CpG-rich *Gad67* (from −840 bp to −768 bp) promoter, the following primers were used: 5′-GAGGAGAGCGGGCCAAGA-3′ (forward) and 5′-GTGCCGCTCCACACGCC-3′ (reverse) (Matrisciano et al., 2013).

Bisulfite sequencing. To determine the methylation pattern of the *Gad67* gene promoter, bisulfite sequencing was performed as previously reported (Chew et al., 2012). Briefly, genomic DNA was extracted using the DNeasy Blood and Tissue kit (QIAGEN). Sodium bisulfite treatment of genomic DNA was performed using an EpiTect Bisulfite kit (QIAGEN), according to the manufacturer's protocol. Following bisulfite treatment, the promoter region of the *Gad67* gene was amplified by PCR using the following primers: 5′-CGTTTAGTAATGTGTTTAAATAT TG-3′ (forward) and 5′-GAACACAACTACCTAACACCACAAA-3′ (reverse). The PCR products were cloned into the pT7 blue vector (Novagen), and at least 8 randomly selected clones were sequenced using the T7 and M13 universal primers.

Measurement of SAM concentration. For measurement of SAM, a commercial ELISA kit (STA-671-C, Cell Biolabs) was used according to the manufacturer's instructions. Briefly, all samples were extracted using cold PBS and centrifuged at 10,000 × *g* for 15 min at 4°C. The supernatant was collected and used for SAM measurement, and the insoluble pellet was suspended in lysis buffer. Protein concentrations were measured using the BCA Protein Assay Kit (Thermo Fisher Scientific). For ELISA measurement, the sample volume was normalized using 100 μg of protein.

Behavioral analysis and methionine (MET) administration schedule. Mice were treated with saline or MET (5.2 mmol/kg, s.c.) twice per day from day 0 to day 5 (6 d). To evaluate changes in spontaneous, cognitive, and anxious behaviors after 6 d of MET treatment, all mice were subjected to the open field test (OFT), hole-board test (HBT), and novel object recognition test (NORT). The experimenters were blinded to the genotype and scored mouse behaviors throughout the analyses. During the behavioral testing period (7–9 d), the mice received saline or MET (5.2 mmol/kg, s.c.) once per day. All behaviors were automatically monitored with a CompACT VAS/DV video-tracking system (Muromachi

Kikai). During all behavioral tests, the total moving distance, total moving time, and velocity were monitored for each group of mice.

The OFT has been used to examine locomotor activity in a novel environment and anxiety (Archer, 1973). The open field arena (40 cm × 40 cm × 30 cm) was divided into 36 squares to indicate the position of the mice. The mice were initially placed in the center of the open field arena, and their behavior was monitored for 5 min. The elapsed time and ambulation in the board area (number of outer squares entered) and the central area (number of inner squares entered) were recorded.

The HBT has been used to examine novelty-seeking behavior and anxiety (File and Wardill, 1975). The mice were placed in a gray acrylic arena (40 cm × 40 cm × 30 cm) with four equidistant floor holes 3 cm in diameter, and the hole-poke activity was scored. The total elapsed time spent in the center, total number of head-dips, head-dip duration, and latency to the first head-dip during the 5 min testing period were recorded.

The NORT, based on the tendency of rodents to discriminate a familiar object from a new object, was used to evaluate cognitive function (Ennaceur et al., 1997). During the acquisition phase, four objects of the same material were placed diagonally in the corners of the chamber for 10 min. One hour after the acquisition-phase training, two objects were replaced with novel objects, and the exploratory behavior was again analyzed for 5 min. After each phase, the objects were thoroughly cleaned with 75% ethanol to prevent odor recognition. Exploration of an object was defined as rearing on the object or sniffing it at a distance of <1 cm, touching it with the nose, or both behaviors. Successful recognition of a previously explored object was reflected by preferential exploration of the novel object. Discrimination of spatial novelty was assessed by comparing the difference between the time of exploration of the novel (right) and familiar (left) objects and the total time spent exploring both objects.

Experimental design and statistical analysis. All values are expressed as the mean ± SEM. Comparisons between two experimental groups (WT vs *Fabp3* KO mice) were performed using unpaired Student's *t* tests. MET treatment analyses and behavioral tests were analyzed using two-way ANOVA, followed by one-way ANOVA for each group and Dunnett's tests. A *p* value <0.05 was considered significant.

Results

FABP3 is highly expressed in PV[+] GABAergic interneurons of the ACC

Our previous studies showed that FABP3 is expressed in the mouse cerebral cortex (Shioda et al., 2010, 2014); however, FABP3-immunopositive (FABP3^{+}) cells have not been identified to date. According to RT-PCR and qPCR of various brain regions, *Fabp3* was highly expressed in the ACC (Fig. 1A; $t_{(10)} = 3.861$, $p < 0.0001$ for mPFC; $t_{(10)} = 9.780$, $p < 0.0001$ for striatum; $t_{(10)} = 6.032$, $p < 0.0001$ for AM, unpaired *t* test vs ACC). Based on immunohistochemistry experiments, FABP3^{+} cells were scattered throughout layers II-VI (Fig. 1B–F) and were negative for the pyramidal cell marker neurogranin (Fig. 1B). Most FABP3^{+} neurons were positive for PV[+], an inhibitory neuron marker, whereas FABP3 was barely detectable in SOM[+] or CR^{+} neurons in the ACC (Fig. 1C–E; Table 1). Moreover, FABP3 was localized to *Gad67* promoter-driven GFP^{+} neurons (Fig. 1F). These results confirm that FABP3 is specifically expressed in PV[+] inhibitory GABAergic interneurons in the ACC.

Fabp3 gene ablation upregulates GAD67 protein and mRNA expression in the ACC

To investigate whether the lack of FABP3 could lead to abnormalities in GABAergic inhibitory interneurons, we examined the number of PV[+], SOM[+], and CR^{+} neurons in the ACC of *Fabp3* KO mice. There were no significant differences in neuron numbers between WT and *Fabp3* KO mice (Fig. 2A; $t_{(6)} = 0.3288$, $p = 0.7434$ for PV; $t_{(10)} = 0.3169$, $p = 0.7532$ for SOM; $t_{(10)} = 0.0325$, $p = 0.9742$ for CR, unpaired *t* test vs WT). The expression of

inhibitory synaptic proteins (GAD67, GAD65, VGAT, GABA$_A$R, and gephyrin) in the ACC was subsequently examined by Western blotting analysis. Notably, levels of GAD67, a rate-limiting enzyme in basal GABA synthesis (Asada et al., 1997), were increased in the ACC of *Fabp3* KO mice compared with those in WT mice, whereas the remaining proteins did not show significant alterations in expression (Fig. 2B; $t_{(10)} = 8.8230$, $p < 0.0001$ for GAD67; $t_{(8)} = 1.3607$, $p = 0.2106$ for GAD65; $t_{(8)} = 1.9252$, $p = 0.0904$ for VGAT; $t_{(8)} = 0.3157$, $p = 0.7603$ for GABA$_A$R; $t_{(9)} = 0.3999$, $p = 0.6985$ for gephyrin, unpaired *t* test). Consistent with this finding, the expression of *Gad67* mRNA (Fig. 2C; $t_{(6)} = 4.8293$, $p < 0.0001$, unpaired *t* test) and concentration of GABA (Fig. 2D; $t_{(10)} = 2.7971$, $p = 0.0189$, unpaired *t* test) were significantly elevated in the ACC of *Fabp3* KO mice, as indicated by qPCR and ELISA, respectively. These changes were not detected in the mPFC ($t_{(6)} = 0.2414$, $p = 0.8153$ for GAD67 protein; $t_{(6)} = 0.7262$, $p = 0.4748$ for *Gad67* mRNA; $t_{(10)} = 0.5738$, $p = 0.5788$ for GABA, unpaired *t* test) or AM ($t_{(6)} = 0.4361$, $p = 0.6780$ for GAD67 protein; $t_{(6)} = 0.8160$, $p = 0.4202$ for *Gad67* mRNA; $t_{(8)} = 0.2470$, $p = 0.8111$ for GABA, unpaired *t* test) of *Fabp3* KO mice (Fig. 2E–G). Moreover, amounts of DA ($t_{(9)} = 0.0927$, $p = 0.9282$, unpaired *t* test) and 5-HT ($t_{(10)} = 0.2092$, $p = 0.8385$, unpaired *t* test) did not exhibit differences between WT and *Fabp3* KO mice (Fig. 2H,I). Together, these results suggest that *Fabp3* ablation in GABAergic interneurons specifically increases GAD67 expression, which consequently enhances inhibitory synaptic transmission in the ACC.

We subsequently examined whether *Fabp3* expression levels are negatively correlated with *Gad67* expression levels in differentiated neuroblastoma Neuro-2A cells, in which *Gad67* is expressed (Manabe et al., 2005; Sato and Shibuya, 2013). In differentiated Neuro-2A cells, the overexpression of *Fabp3* significantly decreased *Gad67* expression levels (Fig. 2J; $t_{(6)} = 4.2862$, $p = 0.0003$, unpaired *t* test). In contrast, siRNA knockdown of *Fabp3* significantly increased *Gad67* expression levels (Fig. 2J; $t_{(6)} = 3.0821$, $p = 0.0054$, unpaired *t* test). These data suggest that FABP3 may negatively modulate *Gad67* expression in a cell-autonomous manner in GABAergic inhibitory neurons.

Enhancement of inhibitory, but not excitatory, synaptic plasticity in *Fabp3* KO mice

To determine whether *Fabp3* ablation directly affects inhibitory synaptic transmission in the ACC, we measured mEPSC/mIPSC using whole-cell voltage-clamp recordings in layer II/III ACC pyramidal neurons prepared from WT or *Fabp3* KO mice after blocking action potential firing with tetrodotoxin. The mEPSC frequency and amplitude were unaffected by *Fabp3* ablation (Fig. 3A–C; $t_{(8)} = 1.1385$, $p = 0.2573$ for frequency; $t_{(8)} = 0.3570$, $p = 0.7218$ for amplitude, unpaired *t* test). Interestingly, in contrast to the mEPSC, the mIPSC frequency was significantly increased in *Fabp3* KO mice compared with that in WT mice (Fig. 3A,B; $t_{(8)} = 10.5217$, $p < 0.0001$, unpaired *t* test) without a change in amplitude (Fig. 3A,C; $t_{(8)} = 1.1242$, $p = 0.2634$, unpaired *t* test); these findings suggest that the loss of FABP3 resulted in a surplus of inhibitory presynaptic transmission. Sequential recordings of the mEPSC and mIPSC from the same ACC pyramidal neuron indicated different responses in WT and KO mice: there was a significant correlation between the mEPSC and mIPSC frequencies of individual pyramidal neurons from *Fabp3* KO but not WT mice (Fig. 3B). Collectively, pyramidal neurons in the ACC of *Fabp3* KO mice received greater inhibitory synaptic input than those of WT mice. Thus, FABP3 may balance the excitatory and
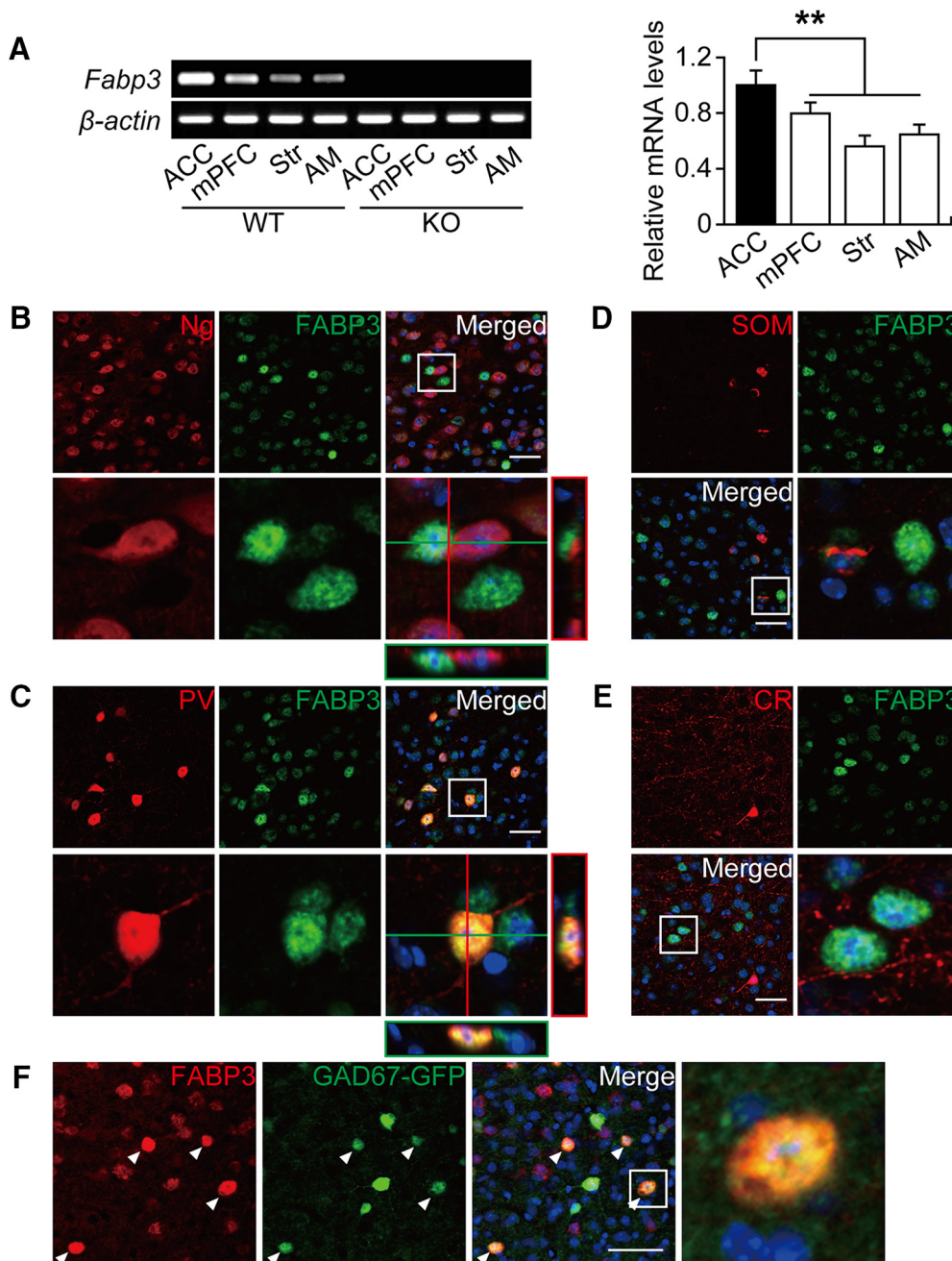
Figure 1. FABP3 was strongly expressed in PV $^+$ GABAergic interneurons of the ACC. **A**, Left, RT-PCR analysis of *Fabp3* in different brain areas. Right, qPCR analysis of *Fabp3* in different brain areas. Error bar indicates mean $\pm$ SEM. $n = 6$ mice per group. **$^{**}p < 0.01$ versus WT ACC. **B–F**, Confocal images showing colocalization of FABP3 and a pyramidal neuronal marker (Ng), three classical GABAergic neuronal makers (PV, SOM, and CR), or GAD67 in the ACC. **B**, Most FABP3 $^+$ structures do not show immunoreactivity for Ng. **C**, Confocal images showing FABP3 and PV colocalization in the ACC. **D, F**, Most FABP $^+$ structures do not show immunoreactivity for SOM (**D**) or CR (**E**). **F**, Confocal images showing FABP3 and GAD67 colocalization in the ACC (arrowheads). **B, C** (bottom), **D**, **E** (bottom right), **F** (right), Enlarged images of the boxed area in the merged image. Scale bars, 50 μm. Str, Striatum.

Table 1. Colocalization of PV, SOM, and CR with FABP3 in the ACC[a]

	PV	SOM	CR
FABP3 $^-$ cell number (per 160 mm^2)	2.3 $\pm$ 0.20	11.1 $\pm$ 0.72	12.4 $\pm$ 0.50
FABP3 $^+$ cell number (per 160 mm^2)	9.5 $\pm$ 0.60	1.2 $\pm$ 0.17	0
Total cell number (per 160 mm^2)	11.7 $\pm$ 0.71	12.3 $\pm$ 0.75	12.4 $\pm$ 0.50
% of FABP3 $^+$	80.6 $\pm$ 1.42	10.3 $\pm$ 1.98	0

[a]Data are mean $\pm$ SEM.

inhibitory inputs to pyramidal neurons through the regulation of GABA synthesis.

Altered glutamatergic transmission in the ACC of *Fabp3* KO mice and expression of glutamatergic synaptic vesicle proteins

We previously demonstrated that *Fabp3* KO mice exhibit dopamine D$_2$ receptor dysfunction and increased glutamate release in the dorsal striatum (Shioda et al., 2010). However, in general, GABA negatively regulates glutamate release through the GABA$_B$ receptor (Bonanno et al., 1997; Isaacson and Hille, 1997; Li et al.,
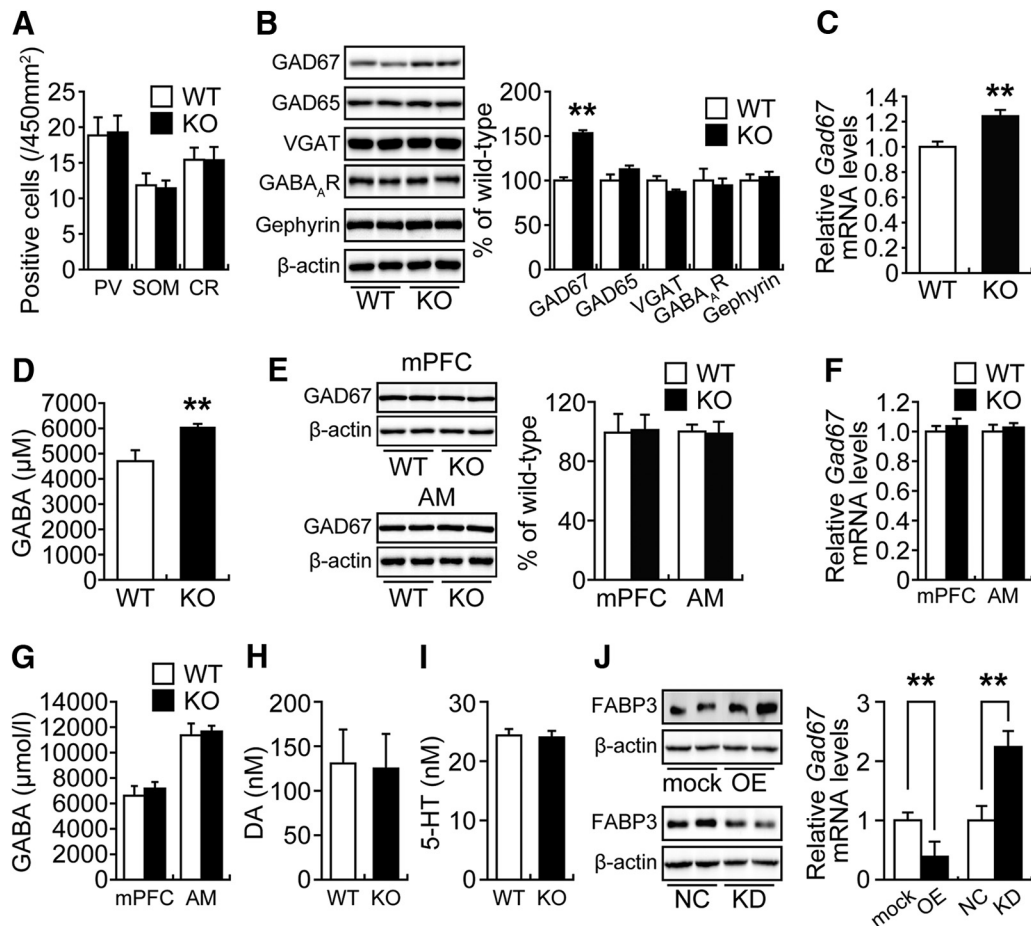
Figure 2. *Fabp3* gene ablation in the ACC caused upregulation of GAD67 expression and GABA synthesis. *A*, Quantitative analysis of the number of PV⁻, SOM⁻, and CR⁺ neurons in the ACC. PV, $n = 8$ sections, 4 mice; SOM, $n = 12$ sections, 6 mice; CR, $n = 12$ sections, 6 mice per group. *B*, Representative immunoblots (left) and quantitative densitometry analysis (right) probed with GABA-related antibodies. GAD67 and β-actin, $n = 6$ mice per group; GAD65, VGAT, and GABA_AR, $n = 5$ mice per group; gephyrin, $n = 5$ and 6 WT and *Fabp3* KO mice, respectively. *C*, Quantitative analysis of *Gad67* mRNA expression in the ACC from WT and *Fabp3* KO mice. $n = 4$ mice per group. *D*, Quantitative analysis of the GABA concentrations in ACC extracts from WT and *Fabp3* KO mice by ELISA. $n = 6$ mice per group. *E–G*, There were no differences in GAD67 expression or GABA synthesis in the mPFC or AM of *Fabp3* KO mice. *E*, Representative immunoblots (left) and quantitative densitometry analysis (right) probed with GAD67 antibody. $n = 4$ mice per group. *F*, Quantitative analysis of the *Gad67* mRNA expression. $n = 4$ mice per group. *G*, Quantitative analysis of the GABA concentrations in the mPFC and AM extracts by ELISA. mPFC, $n = 6$ mice per group; AM, $n = 4$ and 6 WT and *Fabp3* KO mice, respectively. *H, I*, Quantitative analysis of the DA and 5-HT concentrations in ACC extracts by ELISA. 5-HT, $n = 6$ mice per group; DA, $n = 6$ and 5 WT and *Fabp3* KO mice, respectively. *A–I*, **$p < 0.01$ versus WT mice. *J*, Left, Representative immunoblots probed with FABP3 antibody. Right, Quantitative analysis of *Gad67* mRNA in Neuro-2a cells. $n = 4$ per group. **$p < 0.01$ versus control. mock, Mock control; OE, *Fabp3* overexpression; NC, negative control; KD, *Fabp3* knockdown. Error bar indicates mean ± SEM.

2002; Rost et al., 2011; Higley, 2014); thus, it is possible that glutamate release is reduced in the ACC of *Fabp3* KO mice. To confirm this hypothesis, we measured basal and depolarization-induced glutamate release in freely moving mice. As expected, the basal glutamate release was significantly decreased in the ACC of *Fabp3* KO mice compared with that in WT mice (Fig. 4A, left). Area under the curve (AUC) analysis also showed that the basal- and high KCl-evoked glutamate release was significantly decreased in *Fabp3* KO mice (Fig. 4A, right; $t_{(9)} = 2.9984$, $p = 0.0171$ for basal; $t_{(9)} = 2.8990$, $p = 0.0199$ for high K⁺, unpaired *t* test). In addition, the responsiveness of glutamate release to depolarization stimulation was not altered in *Fabp3* KO mice (Fig. 4B; $t_{(9)} = 1.3113$, $p = 0.2261$, unpaired *t* test). Consistent with these findings, the phosphorylation of CaMKIV and CREB and the expression of BDNF, which are indicative of glutamatergic signal transduction, were markedly decreased in the ACC of *Fabp3* KO mice (Fig. 4C; $t_{(10)} = 2.0980$, $p = 0.040$ for pCaMKIV; $t_{(10)} = 2.3883$, $p = 0.0381$ for pCREB; $t_{(10)} = 2.3993$, $p = 0.0374$ for BDNF, unpaired *t* test). To further investigate the effect of *Fabp3* gene ablation on the synaptic profile, we examined the

expression of synaptic proteins (synaptophysin, VGLUT1, and PSD95) in the ACC. Significant increases in the expression of synaptophysin, a general marker for presynaptic vesicle membranes, and VGLUT1, a marker for the glutamatergic presynaptic vesicle, were observed, whereas the expression of PSD95, an excitatory postsynaptic scaffold protein, was not altered (Fig. 4D; $t_{(10)} = 5.7168$, $p = 0.0002$ for synaptophysin; $t_{(10)} = 7.8830$, $p = 0.00001$ for VGLUT1; $t_{(10)} = 0.6290$, $p = 0.5435$ for PSD95, unpaired *t* test).

Decreased binding of MeCP2 and HDAC1 to the *Gad67* promoter region in the ACC of *Fabp3* KO mice

It has been reported that the inhibition of DNMT1 or HDAC1 increases *Gad67* expression (Kundakovic et al., 2007, 2009), which indicates that the DNA methylation and assembly of repressor complexes containing HDAC1 are important for silencing of the *Gad67* promoter. To explore whether the upregulation of *Gad67* expression in the ACC of *Fabp3* KO mice is associated with *Gad67* promoter silencing, the binding of MeCP2 and HDAC1 to specific *Gad67* CpG-rich promoter sequences (−154
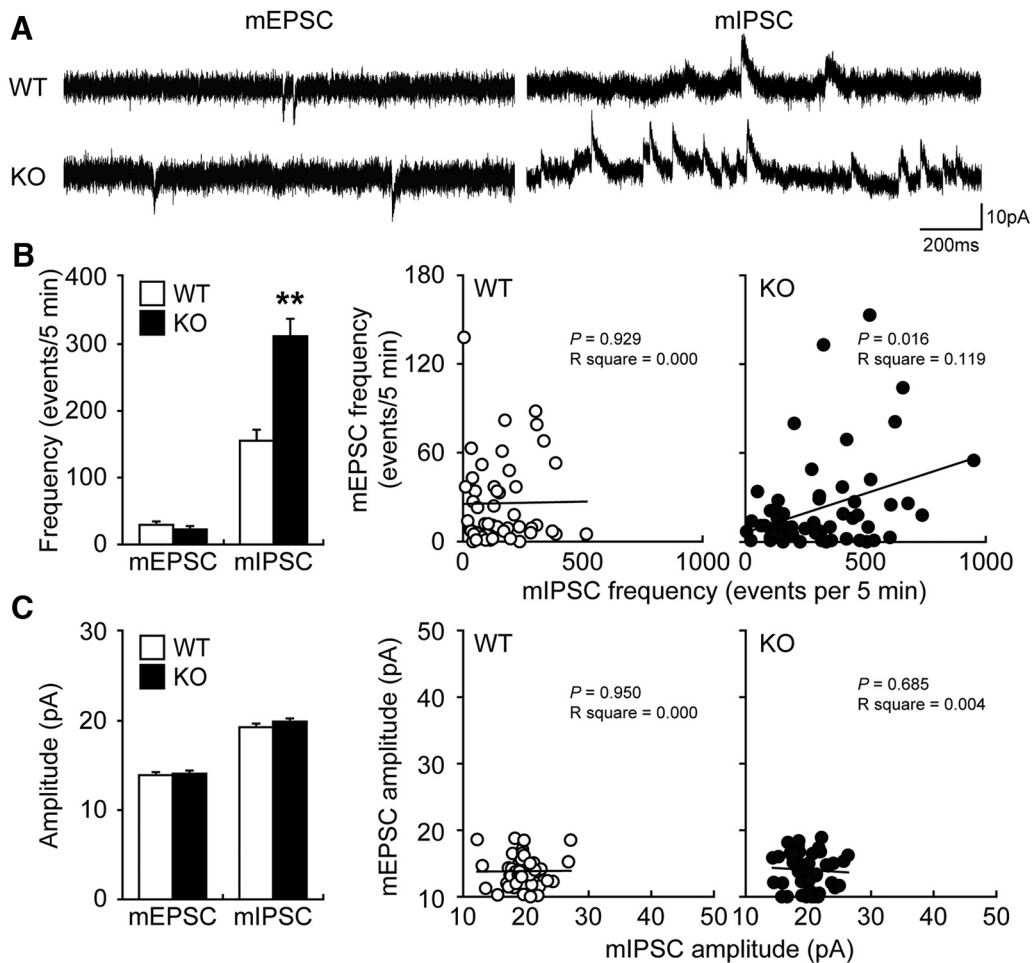
Figure 3. Enhancement of inhibitory synaptic plasticity in the ACC of *Fabp3* KO mice. ***A***, Representative traces of mEPSCs and mIPSCs in ACC layer II/III pyramidal neurons. ***B***, Plots of the mEPSC and mIPSC frequencies in WT and *Fabp3* KO mice. ***C***, Plots of the mEPSC and mIPSC amplitudes in WT and *Fabp3* KO mice. $n = 53$ cells for WT and 59 cells for *Fabp3* KO from 5 mice for mEPSCs. $n = 52$ cells for WT and 60 cells for *Fabp3* KO from 5 mice for mIPSCs. ***p** < 0.01 versus WT mice. Error bar indicates mean ± SEM.

to 21) was examined via ChIP assay. We first confirmed that the expression of MeCP2 and HDAC1 in the ACC was not affected by *Fabp3* deficiency (Fig. 5A; $t_{(10)} = 0.4912$, $p = 0.6407$ for MeCP2; $t_{(10)} = 1.3455$, $p = 0.2271$ for HDAC1, unpaired t test); interestingly, the binding of MeCP2 and HDAC1 to the *Gad67* promoter region was significantly decreased in the ACC of *Fabp3* KO mice (Fig. 5B; $t_{(7)} = 3.9027$, $p = 0.0059$ for MeCP2; $t_{(7)} = 4.2154$, $p = 0.0040$ for HDAC1, unpaired t test).

Chronic MET treatment has previously been reported to downregulate GAD67 expression in the mouse frontal cortex by increasing methylation of the *Gad67* promoter and recruiting MeCP2 to the *Gad67* promoter (Dong et al., 2005, 2007). Therefore, we assessed the effect of methyl donor treatment on the methylation status of the *Gad67* CpG-rich promoter region and the expression of *Gad67* mRNA in the *Fabp3* KO ACC. We determined that the number of methylated cytosine residues at CpG sites in the *Gad67* promoter was decreased in the ACC of *Fabp3* KO mice but was increased after MET treatment for 9 d (Fig. 5C). Consistent with these changes in *Gad67* promoter methylation, MET treatment of *Fabp3* KO mice restored *Gad67* expression in the ACC to levels comparable with that in vehicle-treated WT mice (Fig. 5D; WT: KO, $t_{(9)} = 4.8293$, $p = 0.0003$; KO: KO + MET, $t_{(9)} = 2.9163$, $p = 0.0068$, unpaired t test). We then measured levels of SAM, which is biosynthesized from MET and acts as a direct methyl donor (Szyf, 2015). However, there were no

significant differences in SAM levels in the ACC between WT and *Fabp3* KO mice (Fig. 5E; $t_{(6)} = 1.8038$, $p = 0.1043$, unpaired t test). In contrast, in differentiated Neuro-2A cells, the overexpression of *Fabp3* significantly increased intracellular SAM levels (Fig. 5F; $t_{(6)} = 3.4647$, $p = 0.0033$, unpaired t test).

Amelioration of behavioral abnormalities in *Fabp3* KO mice by chronic MET treatment

As perturbation of the excitatory/inhibitory balance in the ACC leads to behavioral abnormalities, *Fabp3* KO mice were treated with MET and submitted to a behavioral testing battery to evaluate emotional and cognitive functions (Fig. 6A). Based on the OFT, performed to evaluate locomotor activity and anxiety (Archer, 1973), there were no differences in locomotor activity or the time spent in the center area between *Fabp3* KO and WT mice (Fig. 6B; $t_{(32)} = 0.3261$, $p = 0.7464$, unpaired t test). The results of the HBT, performed to evaluate novelty-seeking behavior and anxiety (File and Wardill, 1975), showed that *Fabp3* KO mice spent less time in the center area of the open field and exhibited significantly less head-dipping into the hole than WT mice (Fig. 6C; $t_{(25)} = 4.0959$, $p = 0.0004$ for total center time; $t_{(27)} = 3.7165$, $p = 0.0009$ for head-dip count; $t_{(27)} = 2.8561$, $p = 0.0082$ for head-dip duration; $t_{(27)} = 3.7443$, $p = 0.0009$ for head-dip latency, unpaired t test). Based on the results of the NORT, performed to evaluate cognitive function (Ennaceur et al., 1997), the
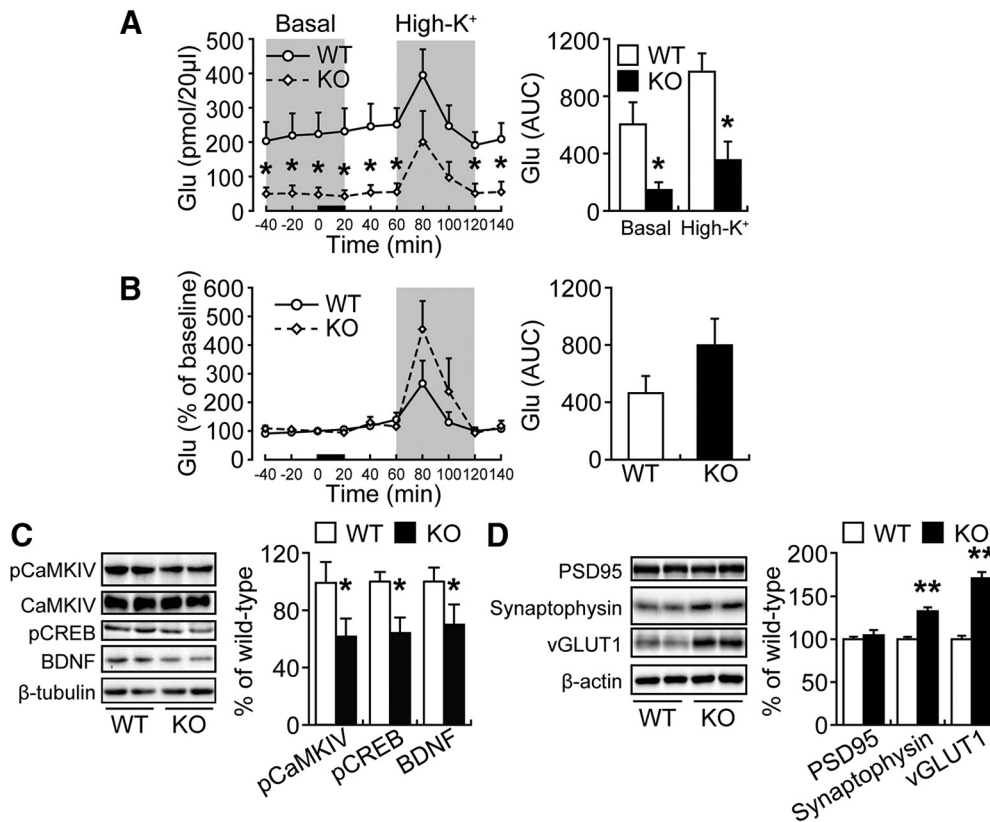
Figure 4. Extracellular glutamate (Glu) concentrations in the ACC in freely moving animals. *A*, Dialysate Glu concentrations at baseline (basal) and after depolarization stimulation (High-K^{+}) (left). Glu AUC before (basal) and after (High-K^{+}) depolarization stimulation (right). $*p < 0.05$ versus wild-type mice. *B*, Normalization of the dialysate Glu signals indicated that the response to depolarization stimulation was enhanced in *Fabp3* KO mice (left). The normalized Glu AUC after depolarization stimulation (right). *A*, *B*, Error bar indicates mean ± SEM. $*p < 0.05$ versus WT mice. $n = 6$ WT mice; $n = 5$ *Fabp3* KO mice. *C*, *D*, Representative immunoblots (left) and quantitative densitometry analysis (right) probed with various antibodies. $*p < 0.05$; $**p < 0.01$ versus WT mice. $n = 6$ mice per group. Error bar indicates mean ± SEM.

discrimination index did not differ between WT and *Fabp3* KO mice in the trial session, but *Fabp3* KO mice failed to discriminate a novel object from a familiar object in the test session (Fig. 6D; $t_{(26)} = 8.4820$, $p < 0.0001$ for WT; $t_{(26)} = 0.9327$, $p = 0.3595$ for *Fabp3* KO, unpaired t test). These results, which are mostly consistent with our previous findings (Shimamoto et al., 2014; Yabuki et al., 2018), indicate that *Fabp3* KO mice show altered cognitive and emotional behaviors.

Finally, we examined whether chronic MET treatment improves the behavioral deficits exhibited by *Fabp3* KO mice. In the OFT, there were no differences in time spent in the center area among the groups following MET treatment (Fig. 6B; WT: WT + MET, $t_{(29)} = 0.3668$, $p = 0.7164$; KO: KO + MET, $t_{(31)} = 0.5350$, $p = 0.5965$, unpaired t test). Moreover, chronic MET treatment of *Fabp3* KO mice significantly improved their impaired explorative behaviors in the HBT (KO: KO + MET, $t_{(24)} = 4.3079$, $p = 0.0002$ for total center time; $t_{(25)} = 4.4016$, $p = 0.0002$ for head-dip count; $t_{(25)} = 4.0482$, $p = 0.0004$ for head-dip duration; $t_{(25)} = 3.4921$, $p = 0.0018$ for head-dip latency, unpaired t test), whereas the behavior of WT mice was not affected by MET treatment (WT: WT + MET, $t_{(25)} = 1.8068$, $p = 0.0829$ for total center time; $t_{(26)} = 0.3319$, $p = 0.7426$ for head-dip count; $t_{(26)} = 0.3178$, $p = 0.7532$ for head-dip duration; $t_{(26)} = 0.4144$, $p = 0.6820$ for head-dip latency, unpaired t test) (Fig. 6C). Last, chronic MET treatment of *Fabp3* KO mice significantly improved the impaired discrimination index during the test session (KO: KO + MET, $t_{(20)} = 4.570$, $p = 0.0002$, unpaired t test), whereas the behavior of WT mice was not affected by MET treat-

ment (WT: WT + MET, $t_{(20)} = 5.7670$, $p = 0.00001$, unpaired t test) (Fig. 6D). There was no significant difference in locomotor activity among the groups during the test (Table 2).

Discussion

In the present study, we identified FABP3 as a negative regulator of *Gad67* mRNA expression in GABAergic interneurons of the ACC. First, we found that FABP3 was exclusively expressed in PV[+] GABAergic inhibitory interneurons in the ACC. Second, increased GAD67 expression, GABA levels, and mIPSC frequency were detected in the ACC of *Fabp3* KO mice. Third, the *Gad67* promoter was hypomethylated, and the binding of transcriptional repressor complexes to the *Gad67* promoter was decreased in the ACC of *Fabp3* KO mice. Finally, normal *Gad67* mRNA expression levels and behaviors exhibited by *Fabp3* KO mice were mostly restored by MET treatment. Based on these observations, we suggest that FABP3 regulates GABA synthesis in GABAergic inhibitory interneurons through transcriptional regulation of *Gad67* in the ACC.

FABP3 was specifically expressed in PV[+] interneurons and not in pyramidal neurons in the ACC. PV[+], SOM[+], and CR^{+} neurons are thought to be constitutively independent neuron groups in the rodent frontal cortex (Hladnik et al., 2014). PV[+] interneurons are the major players that maintain a proper excitatory/inhibitory balance in the CNS. PV[+] interneurons constitute ~40% of GABAergic interneurons in layers II to VI of the frontal cortex, including the ACC (Uematsu et al., 2008), whereas SOM[+] and CR[+] interneurons constitute ~20% and 15%, re-
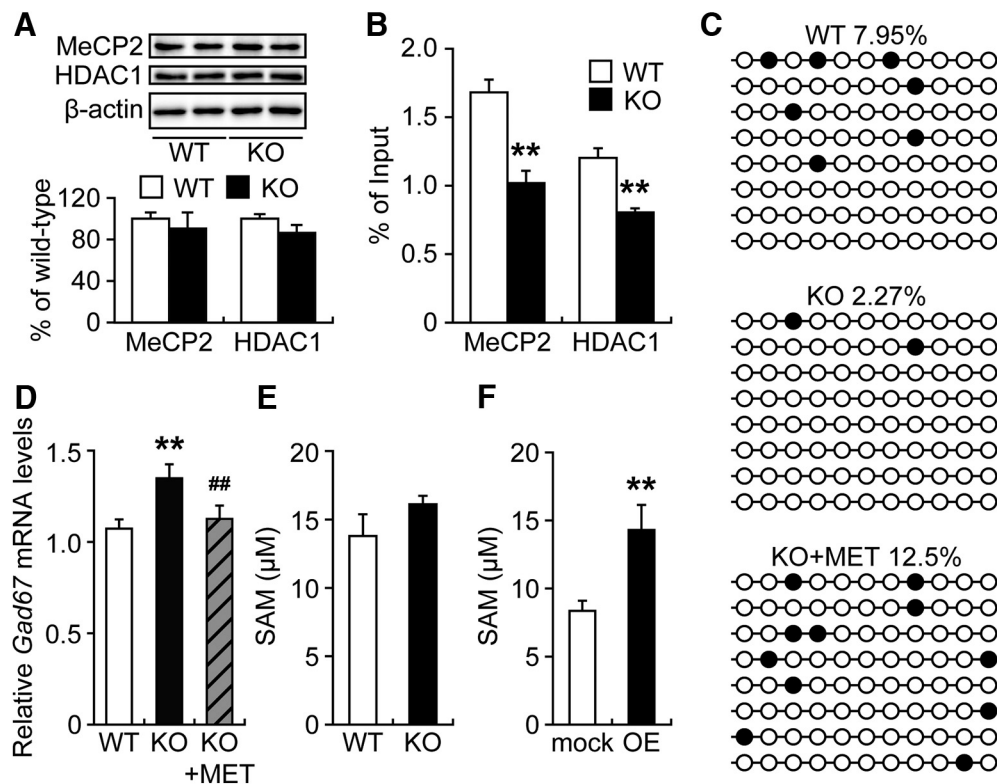
Figure 5. Decreased binding of MeCP2 and HDAC1 to the *Gad67* promoter region in the ACC of *Fabp3* KO mice. ***A***, Representative immunoblots (top) and quantitative densitometry analysis (bottom) probed with various antibodies are shown. $n = 6$ mice per group. ***B***, ChIP assay of ACC extracts from WT or *Fabp3* KO mice via anti-MeCP2 and HDAC1. The precipitated DNA was analyzed by qPCR with primers amplifying the *Gad67* promoter region. **$p < 0.01$ versus WT mice. $n = 5$ WT mice. $n = 4$ *Fabp3* KO mice. ***C***, DNA methylation profile in the *Gad67* promoter region determined by bisulfite sequencing. Black circles represent methylated CpGs. Open circles represent unmethylated sites. Top numbers indicate global percentages of methylated cytosines. ***D***, Quantitative analysis of the *Gad67* mRNA expression in the ACC. WT, $n = 6$; KO, $n = 5$; KO + MET, $n = 6$ mice per group. **$p < 0.01$ versus WT mice. ##$p < 0.01$ versus KO mice. ***E***, ***F***, Quantitative analysis of the SAM concentration by ELISA. $n = 4$ per group. **$p < 0.01$ versus mock control. MET treatment (5.2 mmol/kg, s.c., twice per day for 6 d). mock, Mock control; OE, *Fabp3* overexpression. Error bar indicates mean ± SEM.

spectively. In this study, *Fabp3* ablation did not affect the number of PV$^+$, SOM$^+$, or CR$^+$ interneurons; thus, it is reasonable to assume that the subpopulation of GABA interneurons did not change in *Fabp3* KO mice. Based on our present finding that *Fabp3* ablation significantly increased the GABA concentration in the ACC, it is reasonable to consider that the GABA synthesis capacity per individual PV$^+$ interneuron was increased in the ACC of *Fabp3* KO mice.

GABAergic interneurons are distributed throughout the brain and are the main source of neuronal inhibition in the brain, thus playing a key role in controlling and orchestrating the activity of excitatory pyramidal neurons. Enhanced GABAergic inhibition at the glutamatergic terminal via the GABA$_B$ receptor results in an overall decrease in the basal and depolarization-induced release of glutamate. In general, GABA receptors are classified as ionotropic GABA$_A$ receptors and metabotropic GABA$_B$ receptors. Postsynaptic GABA$_B$ receptor activation inhibits calcium influx at the postsynaptic membrane via VGCCs and the NMDA receptor (Gassmann and Bettler, 2012), consequently silencing the CaMKIV/CREB/BDNF pathway in excitatory pyramidal neurons. In this study, we demonstrated the hypoactivation of pyramidal neurons in the *Fabp3* KO ACC, as indicated by an increase in mIPSC frequency and decrease in basal glutamate release.

Furthermore, the CaMKIV/CREB/BDNF pathway, which is a well-established indicator of neuronal plasticity, was downregulated in the *Fabp3* KO ACC. Thus, increased activation of postsynaptic GABA$_B$ receptors may represent a major cause of the decrease in CaMKIV/CREB/BDNF pathway activity observed in the ACC of *Fabp3* KO mice. By contrast, activation of presynaptic GABA$_B$ receptors inhibits VGCCs, thereby suppressing evoked calcium-dependent neurotransmitter release by inhibiting vesicle fusion to the presynaptic membrane (Gassmann and Bettler, 2012). Thus, the hyperactivation of presynaptic GABA$_B$ receptor may lead to a decrease in spontaneous glutamate release and the accumulation of synaptic vesicles in the *Fabp3* KO ACC. Therefore, this hyperactivation may cause the increase in synaptic vesicle proteins (synaptophysin and VGLUT1) observed in the ACC of *Fabp3* KO mice.

Glutamatergic hypoactivity and hyperactivity in the ACC have been associated with various behavioral alterations in humans and animal models. fMRI studies have shown that changes in neuronal activity in the ACC are apparent in patients with obsessive-compulsive disorder with disturbances in motivation (Bush et al., 2002; Szechtman and Woody, 2004; Fitzgerald et al., 2005). In animal studies, it has been shown that the ACC is closely involved in novel object recognition during a task (Weible et al., 2009, 2012). Specifically, the microinfusion of muscimol, a GABA$_A$ receptor agonist, into the ACC immediately before the retrieval phase decreases exploratory behavior toward novel objects (Pezze et al., 2017). In our present and previous studies, *Fabp3* KO mice exhibited decreased performance in novelty-seeking (Shimamoto et al., 2014; Yabuki et al., 2018). Therefore, we suggest that glutamatergic hypoactivity due to FABP3 deficiency in the ACC underlies the decreased novelty-seeking performance in *Fabp3* KO mice.
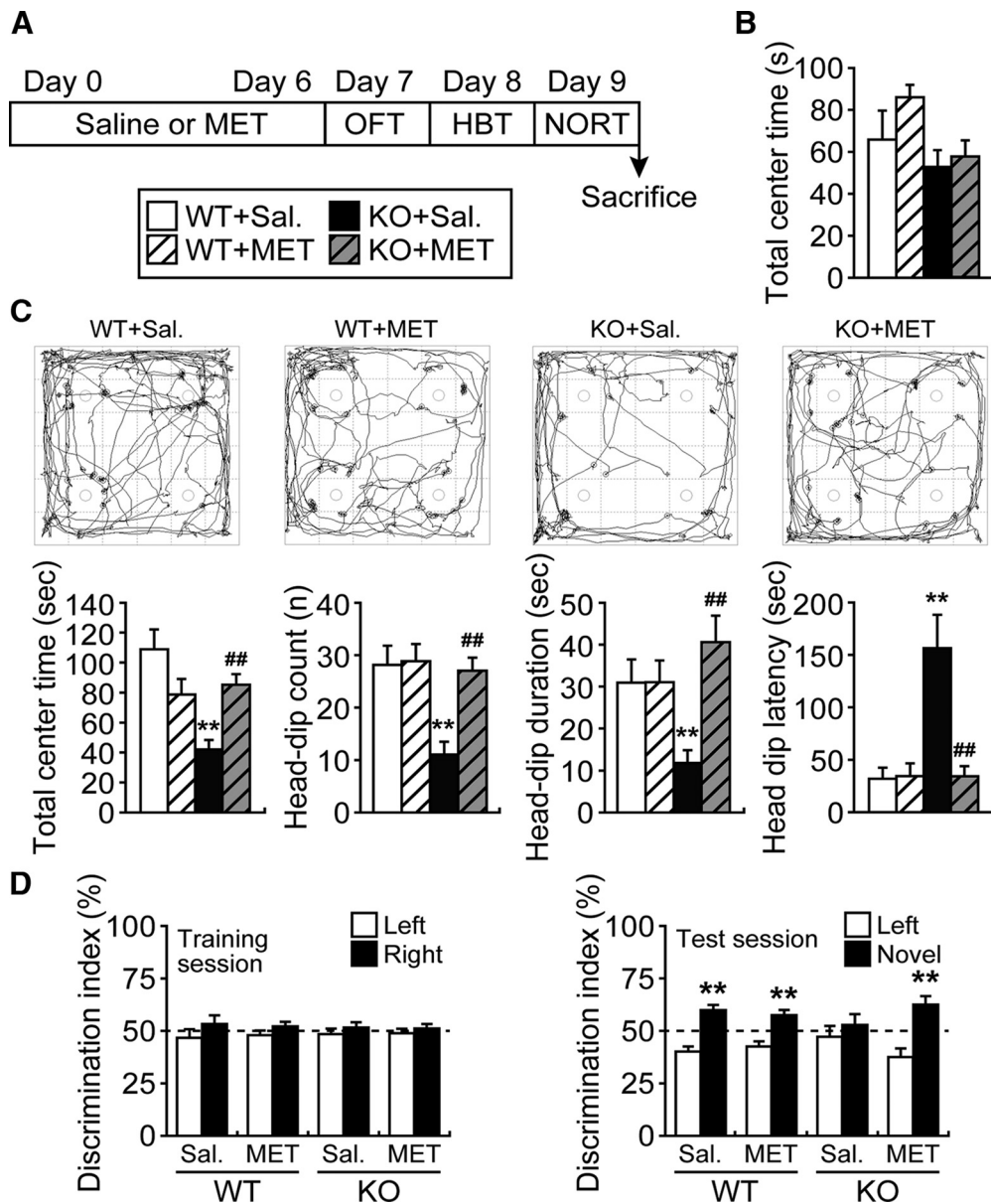
Figure 6. Amelioration of behavioral abnormalities in *Fabp3* KO mice by chronic treatment with MET. ***A***, Schematic of the behavioral tests and MET treatment (5.2 mmol/kg, s.c., twice per day). During the behavioral testing period, mice received saline or MET once per day after testing. ***B***, OFT. Graph represents the time spent in the center area over a 5 min period for WT and *Fabp3* KO mice. $n = 14–17$ mice per group. ***C***, HBT. An illustrative example of the travel pathway in the HBT using video tracking software (top). Graphs represent the time spent in the center area, total number of head-dips, head-dip duration, and latency to first head-dip for the 5 min testing session (bottom). $n = 13–15$ mice per group. **$p < 0.01$ versus saline-treated WT mice. ##$p < 0.01$ versus saline-treated KO mice. ***D***, NORT. Differences in exploratory preference were assessed between groups in the training (left) or test (right) sessions. $n = 11–15$ mice per group. **$p < 0.01$ versus familiar group. Sal, Saline treatment. MET treatment (5.2 mmol/kg, s.c., twice per day for 6 d). Error bar indicates mean ± SEM.

Table 2. Locomotor activities during behavioral tests[a]

Test	Parameter	WT	WT + MET	*Fabp3* KO	*Fabp3* KO + MET
OFT	Total moving distance (cm)	1557.49 ± 151.75	1862.39 ± 154.57	2155.62 ± 202.84	1820.16 ± 64.01
	Total moving time (s)	85.79 ± 6.90	100.74 ± 6.59	107.14 ± 7.24	102.22 ± 2.35
	Velocity (cm/s)	17.73 ± 0.43	18.39 ± 0.60	19.72 ± 0.59	17.75 ± 0.28
HBT	Total moving distance (cm)	1465.62 ± 99.00	1311.54 ± 103.51	1498.69 ± 117.63	1373.93 ± 70.57
	Total moving time (s)	75.88 ± 4.01	70.76 ± 4.65	77.17 ± 5.09	73.03 ± 3.75
	Velocity (cm/s)	19.15 ± 0.55	18.44 ± 0.34	19.18 ± 0.41	18.87 ± 0.35
NORT (Training)	Total moving distance (cm)	2108.58 ± 240.55	1923.98 ± 325.78	2918.21 ± 343.45	2758.50 ± 253.99
	Total moving time (s)	111.72 ± 11.99	106.28 ± 17.45	143.62 ± 13.74	143.53 ± 10.91
	Velocity (cm/s)	18.67 ± 0.43	18.08 ± 0.33	19.67 ± 0.57	19.01 ± 0.33
NORT (Test)	Total moving distance (cm)	1351.41 ± 192.25	934.83 ± 126.64	1271.62 ± 163.09	923.66 ± 137.54
	Total moving time (s)	71.53 ± 9.31	52.43 ± 7.08	69.02 ± 8.63	48.70 ± 5.94
	Velocity (cm/s)	18.76 ± 0.50	17.86 ± 0.24	18.39 ± 0.50	18.49 ± 0.39

[a]Data are mean ± SEM.

In this study, *Gad67* promoter hypomethylation with upregulation of *Gad67* expression was detected in the ACC of *Fabp3* KO mice. Epigenetic modifications are closely associated with various dietary factors, including methyl donors, such as folic acid, vitamin B_{12}, choline, and PUFAs (Milagro et al., 2013). Dietary intake of fish oil rich in docosahexaenoic acid leads to increased levels of MET adenosyl transferase and cystathionine-γ-lyase, key enzymes involved in MET metabolism, in rats (Huang et al., 2010). *n*-3 PUFAs also increase *in vitro* levels of cystathionine-γ-lyase and 5-methyltetrahydrofolate reductase, key enzymes involved in the homocysteine degradation pathway of MET metabolism (Huang et al., 2012). Considering that dietary PUFAs, particularly *n*-6 PUFAs, are transported into the brain by FABP3 (Murphy et al., 2005), it is possible that, through altered MET metabolism, alterations in PUFA uptake and homeostasis in PV$^+$ interneurons of the ACC underlie the epigenetic changes in the *Gad67* promoter and abnormal behaviors in *Fabp3* KO mice. Indeed, *Fabp3* KO mice exhibit reduced incorporation of *n*-6 PUFAs into brain phospholipids (Murphy et al., 2005). Therefore, it is likely that a decrease in *n*-6 PUFA content is associated with epigenetic changes in PV$^+$ interneurons of *Fabp3* KO mice. However, in the current study, we did not observe a reduction in SAM levels in the ACC of *Fabp3* KO mice, although we did find that overexpression of *Fabp3* increased SAM levels in differentiated Neuro-2A cells. Because FABP3 plays an important role in fetal development through the regulation of *n*-3 and *n*-6 PUFA transport (Islam et al., 2014), we speculate that dynamic changes in SAM concentrations may occur during early life stages. In the human cerebral cortex, a robust and progressive rise in DNA methylation levels across the lifespan was observed for the *GAD67* gene, typically in conjunction with declining mRNA levels (Siegmund et al., 2007). Therefore, it is suggested that FABP3 directly regulates MET metabolism, including SAM synthesis, thereby regulating DNA methylation status during the perinatal period. In future studies, we plan to measure DNA methylation and MET metabolism in the ACCs of fetal and juvenile mice.

The present study has an important limitation in that we focused on the methylation status of a single gene promoter, *Gad67*. Indeed, it has been reported that *n*-3 PUFA supplementation leads to changes in the expression of various genes, including calmodulin and protein phosphatase 2A, which play important roles in synaptic plasticity (Kitajka et al., 2002, 2004). In particular, protein phosphatase 2A dephosphorylates CaMKIV and acts as a negative regulator of CaMKIV/CREB signaling (Westphal et al., 1998). Moreover, PUFAs have roles in regulating ion channel activity (Kang and Leaf, 1996; Vreugdenhil et al., 1996). Therefore, FABP3 may indirectly regulate excitatory synaptic plasticity in the brain, including the ACC. Furthermore, prenatal *n*-3 PUFA deficiency increases the DNA methylation of the *Bdnf* promoter in the adult mouse brain (Fan et al., 2016). Therefore, additional studies will be necessary to confirm whether, in addition to the *Gad67* promoter, there are other promoters that are the targets of FABP3 in PV$^+$ interneurons of the ACC.

Protracted treatment with MET successfully reversed *Gad67* promoter hypomethylation in the ACC of *Fabp3* KO mice and their abnormal novelty-seeking behaviors. We showed that chronic MET treatment increased the methylation of the *Gad67* promoter and the binding of repressor complexes, such as MeCP2 and HDAC1, to this region (Dong et al., 2005, 2007). Furthermore, MET treatment in mice affected their social interaction behaviors (Tremolizzo et al., 2005). Although the cellular and molecular mechanisms that underlie how MET treatment restores the phenotypes caused by FABP3 deficiency remain elusive, *Fabp3* KO mice are a useful animal model for exploring the epigenetic involvement in the pathomechanism of various psychiatric diseases with abnormal behaviors.

References

Amemori K, Graybiel AM (2012) Localized microstimulation of primate pregenual cingulate cortex induces negative decision-making. Nat Neurosci 15:776–785. CrossRef Medline

Archer J (1973) Tests for emotionality in rats and mice: a review. Anim Behav 21:205–235. CrossRef Medline

Asada H, Kawamura Y, Maruyama K, Kume H, Ding RG, Kanbara N, Kuzume H, Sanbo M, Yagi T, Obata K (1997) Cleft palate and decreased brain gamma-aminobutyric acid in mice lacking the 67-kDa isoform of glutamic acid decarboxylase. Proc Natl Acad Sci U S A 94:6496–6499. CrossRef Medline

Bali P, Im HI, Kenny PJ (2011) Methylation, memory and addiction. Epigenetics 6:671–674. Medline

Binas B, Danneberg H, McWhir J, Mullins L, Clark AJ (1999) Requirement for the heart-type fatty acid binding protein in cardiac fatty acid utilization. FASEB J 13:805–812. CrossRef Medline

Bonanna G, Fassio A, Schmid G, Severi P, Sala R, Raiteri M (1997) Pharmacologically distinct GABAB receptors that mediate inhibition of GABA and glutamate release in human neocortex. Br J Pharmacol 120:60–64. CrossRef Medline

Bush G, Frazier JA, Rauch SL, Seidman LJ, Whalen PJ, Jenike MA, Rosen BR, Biederman J (1999) Anterior cingulate cortex dysfunction in attention-deficit/hyperactivity disorder revealed by fMRI and the counting stroop. Biol Psychiatry 45:1542–1552. CrossRef Medline

Bush G, Luu P, Posner MI (2000) Cognitive and emotional influences in anterior cingulate cortex. Trends Cogn Sci 4:215–222. CrossRef Medline

Bush G, Vogt BA, Holmes J, Dale AM, Greve D, Jenike MA, Rosen BR (2002) Dorsal anterior cingulate cortex: a role in reward-based decision making. Proc Natl Acad Sci U S A 99:523–528. CrossRef Medline

Chew YC, Adhikary G, Wilson GM, Xu W, Eckert RL (2012) Sulforaphane induction of p21(Cip1) cyclin-dependent kinase inhibitor expression requires p53 and Sp1 transcription factors and is p53-dependent. J Biol Chem 287:16168–16178. CrossRef Medline

Devinsky O, Morrell MJ, Vogt BA (1995) Contributions of anterior cingulate cortex to behaviour. Brain 118:279–306. CrossRef Medline

Di Martino A, Ross K, Uddin LQ, Sklar AB, Castellanos FX, Milham MP (2009) Functional brain correlates of social and nonsocial processes in autism spectrum disorders: an activation likelihood estimation meta-analysis. Biol Psychiatry 65:63–74. CrossRef Medline

Dong E, Agis-Balboa RC, Simonini MV, Grayson DR, Costa E, Guidotti A (2005) Reelin and glutamic acid decarboxylase67 promoter remodeling in an epigenetic methionine-induced mouse model of schizophrenia. Proc Natl Acad Sci U S A 102:12578–12583. CrossRef Medline

Dong E, Guidotti A, Grayson DR, Costa E (2007) Histone hyperacetylation induces demethylation of reelin and 67-kDa glutamic acid decarboxylase promoters. Proc Natl Acad Sci U S A 104:4676–4681. CrossRef Medline

Ebrahimi M, Yamamoto Y, Sharifi K, Kida H, Kagawa Y, Yasumoto Y, Islam A, Miyazaki H, Shimamoto C, Maekawa M, Mitsushima D, Yoshikawa T, Owada Y (2016) Astrocyte-expressed FABP7 regulates dendritic morphology and excitatory synaptic function of cortical neurons. Glia 64:48–62. CrossRef Medline

Elliott E, Manashirov S, Zwang R, Gil S, Tsoory M, Shemesh Y, Chen A (2016) Dnmt3a in the medial prefrontal cortex regulates anxiety-like behavior in adult mice. J Neurosci 36:730–740. CrossRef Medline

Ennaceur A, Neave N, Aggleton JP (1997) Spontaneous object recognition and object location memory in rats: the effects of lesions in the cingulate cortices, the medial prefrontal cortex, the cingulum bundle and the fornix. Exp Brain Res 113:509–519. CrossRef Medline

Fan C, Fu H, Dong H, Lu Y, Qi K (2016) Maternal *n*-3 polyunsaturated fatty acid deprivation during pregnancy and lactation affects neurogenesis and apoptosis in adult offspring: associated with DNA methylation of brain-derived neurotrophic factor transcripts. Nutr Res 36:1013–1021. CrossRef Medline

File SE, Wardill AG (1975) Validity of head-dipping as a measure of exploration in a modified hole-board. Psychopharmacologia 44:53–59. CrossRef Medline

Fitzgerald KD, Welsh RC, Gehring WJ, Abelson JL, Himle JA, Liberzon I,

Taylor SF (2005) Error-related hyperactivity of the anterior cingulate cortex in obsessive-compulsive disorder. Biol Psychiatry 57:287–294. CrossRef Medline

Frankland PW, Bontempi B, Talton LE, Kaczmarek L, Silva AJ (2004) The involvement of the anterior cingulate cortex in remote contextual fear memory. Science 304:881–883. CrossRef Medline

Furuhashi M, Hotamisligil GS (2008) Fatty acid-binding proteins: role in metabolic diseases and potential as drug targets. Nat Rev Drug Discov 7:489–503. CrossRef Medline

Gassmann M, Bettler B (2012) Regulation of neuronal GABA(B) receptor functions by subunit composition. Nat Rev Neurosci 13:380–394. CrossRef Medline

Higley MJ (2014) Localized GABAergic inhibition of dendritic Ca(2+) signalling. Nat Rev Neurosci 15:567–572. CrossRef Medline

Hladnik A, Dzaja D, Darmopil S, Jovanov-Milosevic N, Petanjek Z (2014) Spatio-temporal extension in site of origin for cortical calretinin neurons in primates. Front Neuroanat 8:50. CrossRef Medline

Huang T, Wahlqvist ML, Li D (2010) Docosahexaenoic acid decreases plasma homocysteine via regulating enzyme activity and mRNA expression involved in methionine metabolism. Nutrition 26:112–119. CrossRef Medline

Huang T, Wahlqvist ML, Li D (2012) Effect of *n*-3 polyunsaturated fatty acid on gene expression of the critical enzymes involved in homocysteine metabolism. Nutr J 11:6. CrossRef Medline

Isaacson JS, Hille B (1997) GABA$_B$-mediated presynaptic inhibition of excitatory transmission and synaptic vesicle dynamics in cultured hippocampal neurons. Neuron 18:143–152. CrossRef Medline

Islam A, Kagawa Y, Sharifi K, Ebrahimi M, Miyazaki H, Yasumoto Y, Kawamura S, Yamamoto Y, Sakaguti S, Sawada T, Tokuda N, Sugino N, Suzuki R, Owada Y (2014) Fatty acid binding protein 3 is involved in *n*-3 and *n*-6 PUFA transport in mouse trophoblasts. J Nutr 144:1509–1516. CrossRef Medline

Johansen JP, Fields HL (2004) Glutamatergic activation of anterior cingulate cortex produces an aversive teaching signal. Nat Neurosci 7:398–403. CrossRef Medline

Johansen JP, Fields HL, Manning BH (2001) The affective component of pain in rodents: direct evidence for a contribution of the anterior cingulate cortex. Proc Natl Acad Sci U S A 98:8077–8082. CrossRef Medline

Kang JX, Leaf A (1996) Evidence that free polyunsaturated fatty acids modify Na$^+$ channels by directly binding to the channel proteins. Proc Natl Acad Sci U S A 93:3542–3546. CrossRef Medline

Kasahara J, Fukunaga K, Miyamoto E (1999) Differential effects of a calcineurin inhibitor on glutamate-induced phosphorylation of Ca^{2+}/calmodulin-dependent protein kinases in cultured rat hippocampal neurons. J Biol Chem 274:9061–9067. CrossRef Medline

Kida H, Tsuda Y, Ito N, Yamamoto Y, Owada Y, Kamiya Y, Mitsushima D (2016) Motor training promotes both synaptic and intrinsic plasticity of layer II/III pyramidal neurons in the primary motor cortex. Cereb Cortex 26:3494–3507. CrossRef Medline

Kitajka K, Puskás LG, Zvara A, Hackler L Jr, Barceló-Coblijn G, Yeo YK, Farkas T (2002) The role of *n*-3 polyunsaturated fatty acids in brain: modulation of rat brain gene expression by dietary *n*-3 fatty acids. Proc Natl Acad Sci U S A 99:2619–2624. CrossRef Medline

Kitajka K, Sinclair AJ, Weisinger RS, Weisinger HS, Mathai M, Jayasooriya AP, Halver JE, Puskás LG (2004) Effects of dietary omega-3 polyunsaturated fatty acids on brain gene expression. Proc Natl Acad Sci U S A 101:10931–10936. CrossRef Medline

Kundakovic M, Chen Y, Costa E, Grayson DR (2007) DNA methyltransferase inhibitors coordinately induce expression of the human reelin and glutamic acid decarboxylase 67 genes. Mol Pharmacol 71:644–653. CrossRef Medline

Kundakovic M, Chen Y, Guidotti A, Grayson DR (2009) The reelin and GAD67 promoters are activated by epigenetic drugs that facilitate the disruption of local repressor complexes. Mol Pharmacol 75:342–354. CrossRef Medline

Li DP, Chen SR, Pan YZ, Levey AI, Pan HL (2002) Role of presynaptic muscarinic and GABA(B) receptors in spinal glutamate release and cholinergic analgesia in rats. J Physiol 543:807–818. CrossRef Medline

Liu RZ, Li X, Godbout R (2008) A novel fatty acid-binding protein (FABP) gene resulting from tandem gene duplication in mammals: transcription in rat retina and testis. Genomics 92:436–445. CrossRef Medline

Manabe T, Tatsumi K, Inoue M, Matsuyoshi H, Makinodan M, Yokoyama S,

Wanaka A (2005) L3/Lhx8 is involved in the determination of cholinergic or GABAergic cell fate. J Neurochem 94:723–730. CrossRef Medline

Matrisciano F, Tueting P, Dalal I, Kadriu B, Grayson DR, Davis JM, Nicoletti F, Guidotti A (2013) Epigenetic modifications of GABAergic interneurons are associated with the schizophrenia-like phenotype induced by prenatal stress in mice. Neuropharmacology 68:184–194. CrossRef Medline

Milagro FI, Mansego ML, De Miguel C, Martínez JA (2013) Dietary factors, epigenetic modifications and obesity outcomes: progresses and perspectives. Mol Aspects Med 34:782–812. CrossRef Medline

Miller CA, Gavin CF, White JA, Parrish RR, Honasoge A, Yancey CR, Rivera IM, Rubio MD, Rumbaugh G, Sweatt JD (2010) Cortical DNA methylation maintains remote memory. Nat Neurosci 13:664–666. CrossRef Medline

Mitsushima D, Sano A, Takahashi T (2013) A cholinergic trigger drives learning-induced plasticity at hippocampal synapses. Nat Commun 4:2760. CrossRef Medline

Murphy EJ, Owada Y, Kitanaka N, Kondo H, Glatz JF (2005) Brain arachidonic acid incorporation is decreased in heart fatty acid binding protein gene-ablated mice. Biochemistry 44:6350–6360. CrossRef Medline

Owada Y, Yoshimoto T, Kondo H (1996) Spatio-temporally differential expression of genes for three members of fatty acid binding proteins in developing and mature rat brains. J Chem Neuroanat 12:113–122. CrossRef Medline

Paxinos G, Franklin KBJ (2004) The mouse brain in stereotaxic coordinates. Cambridge, MA: Academic Press.

Pezze MA, Marshall HJ, Fone KC, Cassaday HJ (2017) Role of the anterior cingulate cortex in the retrieval of novel object recognition memory after a long delay. Learn Mem 24:310–317. CrossRef Medline

Rost BR, Nicholson P, Ahnert-Hilger G, Rummel A, Rosenmund C, Breustedt J, Schmitz D (2011) Activation of metabotropic GABA receptors increases the energy barrier for vesicle fusion. J Cell Sci 124:3066–3073. CrossRef Medline

Sato A, Shibuya H (2013) WNK signaling is involved in neural development via Lhx8/Awh expression. PLoS One 8:e55301. CrossRef Medline

Shimamoto C, Ohnishi T, Maekawa M, Watanabe A, Ohba H, Arai R, Iwayama Y, Hisano Y, Toyota T, Toyoshima M, Suzuki K, Shirayama Y, Nakamura K, Mori N, Owada Y, Kobayashi T, Yoshikawa T (2014) Functional characterization of FABP3, 5 and 7 gene variants identified in schizophrenia and autism spectrum disorder and mouse behavioral studies. Hum Mol Genet 23:6495–6511. CrossRef Medline

Shioda N, Yamamoto Y, Watanabe M, Binas B, Owada Y, Fukunaga K (2010) Heart-type fatty acid binding protein regulates dopamine D2 receptor function in mouse brain. J Neurosci 30:3146–3155. CrossRef Medline

Shioda N, Yabuki Y, Kobayashi Y, Onozato M, Owada Y, Fukunaga K (2014) FABP3 protein promotes alpha-synuclein oligomerization associated with 1-methyl-1,2,3,6-tetrahydropiridine-induced neurotoxicity. J Biol Chem 289:18957–18965. CrossRef Medline

Siegmund KD, Connor CM, Campan M, Long TI, Weisenberger DJ, Biniszkiewicz D, Jaenisch R, Laird PW, Akbarian S (2007) DNA methylation in the human cerebral cortex is dynamically regulated throughout the life span and involves differentiated neurons. PLoS One 2:e895. CrossRef Medline

Stadler C, Sterzer P, Schmeck K, Krebs A, Kleinschmidt A, Poustka F (2007) Reduced anterior cingulate activation in aggressive children and adolescents during affective stimulation: association with temperament traits. J Psychiatr Res 41:410–417. CrossRef Medline

Szechtman H, Woody E (2004) Obsessive-compulsive disorder as a disturbance of security motivation. Psychol Rev 111:111–127. CrossRef Medline

Szyf M (2015) Prospects for the development of epigenetic drugs for CNS conditions. Nat Rev Drug Discov 14:461–474. CrossRef Medline

Tamamaki N, Yanagawa Y, Tomioka R, Miyazaki J, Obata K, Kaneko T (2003) Green fluorescent protein expression and colocalization with calretinin, parvalbumin, and somatostatin in the GAD67-GFP knock-in mouse. J Comp Neurol 467:60–79. CrossRef Medline

Tremolizzo L, Doueiri MS, Dong E, Grayson DR, Davis J, Pinna G, Tueting P, Rodriguez-Menendez V, Costa E, Guidotti A (2005) Valproate corrects the schizophrenia-like epigenetic behavioral modifications induced by methionine in mice. Biol Psychiatry 57:500–509. CrossRef Medline

Uematsu M, Hirai Y, Karube F, Ebihara S, Kato M, Abe K, Obata K, Yoshida S, Hirabayashi M, Yanagawa Y, Kawaguchi Y (2008) Quantitative chem-

ical composition of cortical GABAergic neurons revealed in transgenic venus-expressing rats. Cereb Cortex 18:315–330. CrossRef Medline

Vreugdenhil M, Bruehl C, Voskuyl RA, Kang JX, Leaf A, Wadman WJ (1996) Polyunsaturated fatty acids modulate sodium and calcium currents in CA1 neurons. Proc Natl Acad Sci U S A 93:12559–12563. CrossRef Medline

Watanabe K, Wakabayashi H, Veerkamp JH, Ono T, Suzuki T (1993) Immunohistochemical distribution of heart-type fatty acid-binding protein immunoreactivity in normal human tissues and in acute myocardial infarct. J Pathol 170:59–65. CrossRef Medline

Weible AP, Rowland DC, Pang R, Kentros C (2009) Neural correlates of novel object and novel location recognition behavior in the mouse anterior cingulate cortex. J Neurophysiol 102:2055–2068. CrossRef Medline

Weible AP, Rowland DC, Monaghan CK, Wolfgang NT, Kentros CG (2012) Neural correlates of long-term object memory in the mouse anterior cingulate cortex. J Neurosci 32:5598–5608. CrossRef Medline

Westphal RS, Anderson KA, Means AR, Wadzinski BE (1998) A signaling complex of Ca^{2+}-calmodulin-dependent protein kinase IV and protein phosphatase 2A. Science 280:1258–1261. CrossRef Medline

Yabuki Y, Takahata I, Matsuo K, Owada Y, Fukunaga K (2018) Ramelteon improves post-traumatic stress disorder-like behaviors exhibited by fatty acid-binding protein 3 null mice. Mol Neurobiol 55:3577–3591. CrossRef Medline

Yamamoto Y, Shioda N, Han F, Moriguchi S, Nakajima A, Yokosuka A, Mimaki Y, Sashida Y, Yamakuni T, Ohizumi Y, Fukunaga K (2009) Nobiletin improves brain ischemia-induced learning and memory deficits through stimulation of CaMKII and CREB phosphorylation. Brain Res 1295:218–229. CrossRef Medline

Yamamoto Y, Shioda N, Han F, Moriguchi S, Fukunaga K (2013) Novel cognitive enhancer ST101 enhances acetylcholine release in mouse dorsal hippocampus through T-type voltage-gated calcium channel stimulation. J Pharmacol Sci 121:212–226. CrossRef Medline